Advances in Aircraft and Spacecraft Science, *Vol. 11, No. 2 (2024) 153-175*
https://doi.org/10.12989/aas.2024.11.2.153

Heat transfer characteristics of an internal cooling channel with pin-fins and ribbed endwalls in gas turbine blade

Vu T.A. Co[1a], Hung C. Hoang[2b], Duy C.K. Do[2c], Son H. Truong[2d], Diem G. Pham[2e], Nhung T.T. Le[2f], Truong C. Dinh[2g] and Linh T. Nha*[2]

[1]*Vietnam Aviation Academy, No. 104, Nguyen Van Troi Street, Ward 8, Phu Nhuan District, Ho Chi Minh City, Vietnam*
[2]*School of Mechanical Engineering, Hanoi University of Science and Technology, No. 1, Dai Co Viet Road, Hai Ba Trung District, Hanoi 11615, Vietnam*

(Received February 18, 2024, Revised August 6, 2024, Accepted August 9, 2024)

Abstract. In jet engines, turbine blade cooling has an extremely important role. The pin-fin array, which is situated close to the trailing edge of the blade, aids in internal cooling of the gas turbine blades and preserves the structural integrity of the blade. Previous studies often focused on pin-fin configurations, but the current research focuses on improving the geometry at the endwalls to reduce wake vortices behind the pin-fins and enhance heat transfer at the endwalls location. Using the k-ω turbulence model, a numerical study was conducted on a ribbed shape situated on the walls between pin-fin arrays, spanning a Reynolds number range of 7400 to 36000, in order to determine the heat transport characteristics. The heat transfer efficiency coefficient and Nusselt number increase dramatically with the revised wall configuration, according to the numerical data. The channel's heat transfer efficiency is increased by enlarging the heat transfer areas near the pin-fins and by the interaction of the flow with the endwalls. The addition of ribs causes the Nusselt number of the new model to climb from 78% to 96% at the previously given Reynolds numbers, and the heat transfer efficiency index to rise from 60% to 73%. The height (Hr), position (Lr), forward width (Wf), and backward width (Wb) of the ribs are among the geometric elements that were looked at in order to determine how they affected the performance of heat transmission. In comparison to the reference design, the parametric study results demonstrate that the best forward width (Wf/R=18.75%) and backward width (Wb/R=31.25%) increase the heat transfer efficiency index by 0.4% and 1.3%, respectively.

Keywords: gas turbine blade; heat transfer efficiency index; nusselt number; pin-fin internal cooling; RANS analysis; ribbed endwalls

*Corresponding author, Ph.D., E-mail: linh.nhatuong@hust.edu.vn
[a]Ph.D., E-mail: vucotananh@gmail.com
[b]Engineering Student, E-mail: hung.hc184886@sis.hust.edu.vn
[c]Master Student, E-mail: docongkhanhduy@gmail.com
[d]Associate Professor, E-mail: son.truonghoanh@hust.edu.vn
[e]Ph.D., E-mail: diem.phamgia@hust.edu.vn
[f]Ph.D., E-mail: nhung.lethituyet@hust.edu.vn
[g]Ph.D., E-mail: truong.dinhcong@hust.edu.vn

http://www.techno-press.org/?journal=aas&subpage=7 ISSN: 2287-528X (Print), 2287-5271 (Online)

1. Introduction

In the modern aerospace industry, development of turbine engines is at the forefront. Increasing the turbine stage's input temperature is one method used to boost a turbine engine's output and thrust simultaneously. However, if a turbine blade works above the permissible temperature of the material, it leads to thermal melting which reduces the life of the blade. Therefore, methods of cooling turbine blades are a matter of interest to scientists. An effective method involves cooling the inside of the turbine blade by bleeding cool gas from the compressor and subsequently pumping it into the stages located within the turbine blade. The trailing edge domain is one of the cooling zones that is most frequently researched. A common technology to enhance heat transfer in this area is pin-fin arrays. Aerospace Propulsion Systems Laboratory (APSLab.) Pham *et al.* (2020), Dinh *et al.* (2021), Dinh *et al.* (2023), Tran *et al.* (2023) looked at some new internal cooling channel designs on the heat transfer characteristics in an effort to boost the channel's heat transfer capacity. Metzger *et al.* (1982) conducted one of the first investigations of pin-fin arrays on cooling in turbine blades. In comparison to the flat channel, the heat transmission coefficient increased by around double, according to the data. After examining the individual effects of the pins on the channel's overall heat transfer, Zukauskas (1972) cames to the conclusion that the pin surface was the primary source of heat transfer contribution. Sparrow *et al.* (1980) conducted experiments and comparisons between staggered and aligned pin-fin arrays in terms of heat transmission properties. In general, the staggered arrays' heat transfer coefficients were larger than those of the in-line arrays. After comparing the pin-fin spacing of a staggered array with that of other arrays, Siw *et al.* (2015) showed that the staggered array provided a higher heat transfer coefficient and a larger friction factor

The interaction between the flow with the pin-fin's surfaces determines the heat transfer characteristics of a channel with pin-fins. Sircar *et al.* (2020), Kirkil and Constantinescu (2015) investigated the vortex pattern surrounding a cylindrical pin placed on a plate. At the endwalls and behind the pin-fins, they examined the characteristics of the primary, local, and secondary necklace vortices. It is thought that as the flow travels through the pin-fin arrays, the interactions between these vortices represent the properties of the main flow. To ascertain the properties of heat transfer, the interaction between the flow and the pin-fins was also investigated. Otto *et al.* (2019), Won *et al.* (2004) studied vortex shedding in von Kármán vortex systems and Horseshoe vortex systems, among other complex flow patterns. The features of local and global heat transport over the endwall were directly impacted by each of these structures. Additionally, it was discovered that because of enhanced flow instabilities that encourage shear layer separation and vortex generation, the vortex shape differs dramatically between the two Reynolds values. More research was done on the pin-fin vortices by Schekman and Kim (2017), Sahin *et al.* (2008). They discovered that the interaction of these vortices with the pin-fins was what produced the heat transfer characteristic of the pin-fin arrays.

The cross-sectional shape of a pin-fin is thought to be a key component influencing its ability to transmit heat in a channel. The turbulence-related pin-fin flow mechanism varies with changes in the cross section, which impacts the channel's heat transfer properties (Ghosh *et al.* 2020). The ideal pin-fin cross-sectional shape has also been the subject of pin-fin investigations. The cross-section types that have been explored include fan-shaped (Moon and Kim 2013), elliptical (Li and Kim 2008), circular, cubic (Sahiti *et al.* 2006), and diamond (Wan *et al.* 2017). According to these researches of Sahiti *et al.* (2006), Wan *et al.* (2017), Li and Kim (2008), Moon and Kim (2013), angled cross-sections increase heat transfer but come with significant pressure losses.

The pin-fin height and pin-fin arrays spanwise spacing, also known as the ratio of the height to diameter (H/D) and the ratio of the distance between the pin-fins to the diameter (S/D), are significant additional elements that draw a lot of attention from researchers worldwide. The research of Axtmann *et al.* (2016) shown that arrays with shorter pin-fins enhanced heat transfer more. Additionally, a higher heat transfer efficiency for the channel may be discovered with the appropriate combination of H/D and S/D (Ostanek and Thole 2012, Park *et al.* 2008, Chyu *et al.* 2009). Brigham and VanFossen (1984) shown that Nusselt number was dependent on Reynolds number and H/D for longer pin-fins. Regarding H/D<2, the channel's heat transfer capacity was solely determined by the Reynolds number. Pin-fins with gaps (Sa and Kim 2015, Sa *et al.* 2016), detachable pin-fins (Ye *et al.* 2017, Chi *et al.* 2011, Liang and Rao 2012), and pin-fins with endwall fillets (Chyu 1990) were all the subject of several studies. The results of these investigations demonstrate that when the gaps' sizes increase and the flow resistance progressively drops, the heat transfer coefficient and the friction coefficient also decrease. Higher heat transfer efficiency is achieved, nevertheless, because the decreased pressure loss outweighs the decreased heat transmission.

The studies stated above are all concerned with the pin-fin's profile shape and its changes in dimensions, which include height and diameter. Understanding flow and vortex dynamics to improve the heat transfer properties of channels with pin-fins was the shared goal of these investigations. On the other hand, Tang *et al.* (2020) demonstrated that the channel's primary locations for enhanced heat transmission were discovered to be upstream and in the vicinity of the turbulator. By comparing the effects of circular and fan-shaped pin-fins, Moon and Kim (2023) demonstrated that the wake zone behind the pin-fin had the lowest Nusselt number. Additionally, the fan-shape helped to reduce this area and raise the channel's heat transfer capacity. Uzol and Camci (2001) contrasted the elliptical and circular pin-fins' heat transfer properties. The findings demonstrated that the pressure loss through the circular pin-fin was more than that via the elliptical pin-fin due to the separation of flow flowing through it. An elliptical pin-fin with a higher Heat Transfer Efficiency Index was the outcome of this. A topic of recent interest is how endwalls affect heat transport in a channel with pin-fins.

The impact of recessed and extruded endwalls on the heat transmission properties of pin-fin arrays was recently examined by Do *et al.* (2022). The findings demonstrated that, in order to improve the channel's heat transmission properties, the endwalls assisted in altering the vortex's structure through the pin-fins and reducing the wake region behind them. Based on this, the current numerical study examines the effects of ribbed and flat endwalls on the properties of heat transmission in a cooling channel featuring rows of pin-fins. The endwalls in this work are innovative because of their new configuration, namely the square ribs that are sandwiched between pin-fin rows. Additionally, a parametric research is conducted to determine the impact on heat transmission of the ribbed endwall shape.

2. Numerical analysis

2.1 Geometric configuration

The computational domain, based on the experimental model of Bai *et al.* (2019), is depicted in Fig. 1. The developing channel (L_d), ribbed channel (L_p), heated channel (L), and outlet channel (L_0) are the four components of the rectangular channel computational model. There are four

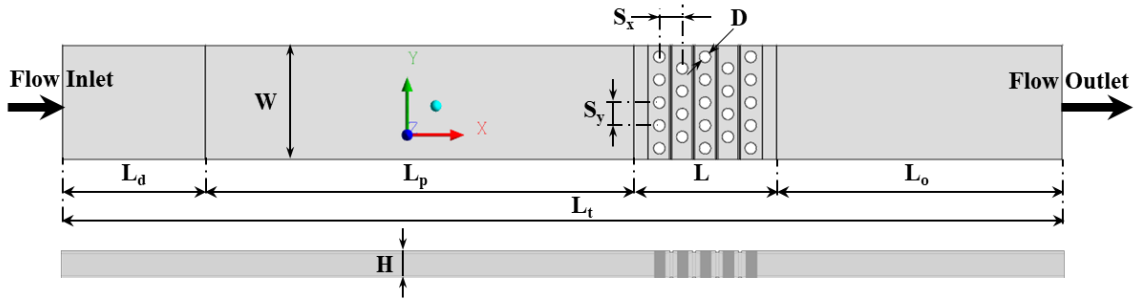

(a) Geometric configurations

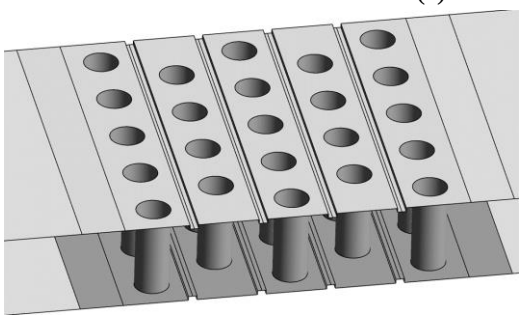

(b) 3D pin-fins with ribbed endwalls

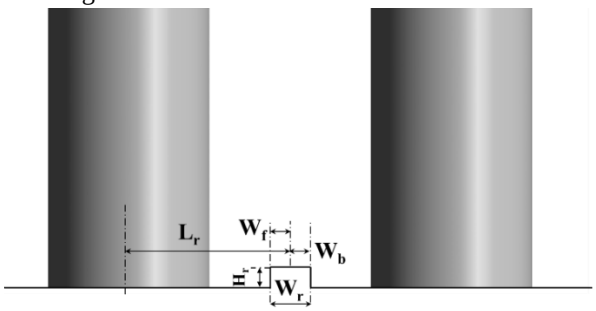

(c) Design parameters of ribbed endwall

Fig. 1 Geometric configurations of cooling channel with pin-fins and ribbed endwalls

Table 1 Geometric parameters of ribbed endwalls

Parameter	H_r/H	L_r/R	W_f/R	W_b/R
Reference design	10%	200%	25%	25%
Min.	5.0%	150%	6.25%	6.25%
Max.	20%	250%	43.75%	43.75%
Steps	2.5%	12.5%	6.25%	6.25%

spanwise square ribs and five staggered pin-fins rows in the heated channel. It is believed that the ribbed channel is a basic heated channel. W=80 mm and H=20 mm are the overall channel height and width, respectively. The computational domain's cross section has a rectangular shape with the aspect ratio $AR=W/H=4$. The other two walls are located at $y=-W/2$ and $y=W/2$, while the above and bottom walls are located at coordinates $z=0$ and $z=H$, respectively. $D_h=2WH/(H+W)=32$ mm is the channel's equivalent hydraulic diameter. The direction of the flow matches the x-axis direction. The inflow is stabilized in Fig. 1 by the development channel length, L_d=100 mm, which is computed from the inlet. Lp=300 mm is the ribbed channel length, while L=100 mm is the length of the heated channel. L_0=200 mm is the outlet channel's calculated length measured to the channel's end. The effective reduction of backflow is the goal of this channel. The channel's total length is Lt=700 mm. The pin-fin spacings in the heated channel (spanwise direction) are S_y/D=2 and S_x/D=2, and a diameter of D=8 mm for each pin-fin.

The purpose of this study is to improve the vortex area surrounding the pin-fins by using ribbed endwalls in the pin-fin rows. Fig. 1(b) and 1(c) depict the geometric configuration of ribbed endwalls. In the middle of two adjacent pin-fin rows on the endwalls are the rib rows. The height

of the ribs is between 5% and 10% of the hydraulic diameter of the channel, according to the majority of earlier articles Pham *et al.* (2020), Dinh *et al.* (2022), Bai *et al.* (2019) on the use of ribs to improve heat exchange in turbine blades. For this reason, 6.25% is the height ratio used for the current task. Therefore, the ribs' *z-x* cross-section is a square with W_f=W_b=1mm and H_r=W_r=2 mm. The ribbed endwalls' precise geometric specifications are displayed in Tab. 1. In order to determine the best design, these variables are adjusted in order to assess the pin-fin arrays' heat transmission propertie.

2.2 Performance parameters

The definition of Reynolds number (*Re*) is as follows

$$Re = \frac{\rho u D_h}{\mu} \tag{1}$$

where ρ, μ, *u*, and *Dh* stand for the channel's hydraulic diameter, inflow velocity, coolant density, and dynamic viscosity, respectively.

The following is the definition of the local heat transfer coefficient (*h*)

$$h = \frac{q}{T_w - T_b} \tag{2}$$

where the wall heat flux, fluid's wall temperature, and bulk temperature are represented by the numbers *q*, *Tw* and *Tb*, respectively. According to the formula of Bai *et al.* (2019), *Tb* is interpolated along the streamwise direction based on *x* location.

The local heat transfer coefficient (h) is computed using the local Nusselt number (*Nu*)

$$Nu = \frac{h.D_h}{\lambda} \tag{3}$$

where λ is the fluid coolant's thermal conductivity.

The Nusselt number (Nu_0) for fully developed turbulent flow in a smooth channel is defined as follows, based on the Dittus-Boelter (1985) correlation

$$Nu_0 = 0.023.Re^{0.8}Pr^{0.4} \tag{4}$$

where Pr is Prandtl number.

The definition of the channel's friction factor with pin-fins is

$$f = \frac{\Delta P D_h}{2\rho L u^2} \tag{5}$$

where ΔP and *L* are pressure drop across the heated channel and length of the heated channel.

In a smooth channel, the friction factor obtained for fully developed flow is given as follows

$$f_0 = 0.316Re^{-0.25} \tag{6}$$

The heat tranfer efficiency index (HTEI) is defined as

$$\eta = \left(\frac{\overline{Nu}}{Nu_o}\right) / \left(\frac{f}{f_o}\right)^{1/3} \tag{7}$$

where the average Nusselt number over the upper and lower heated endwalls is represented by $\overline{Nu}$.

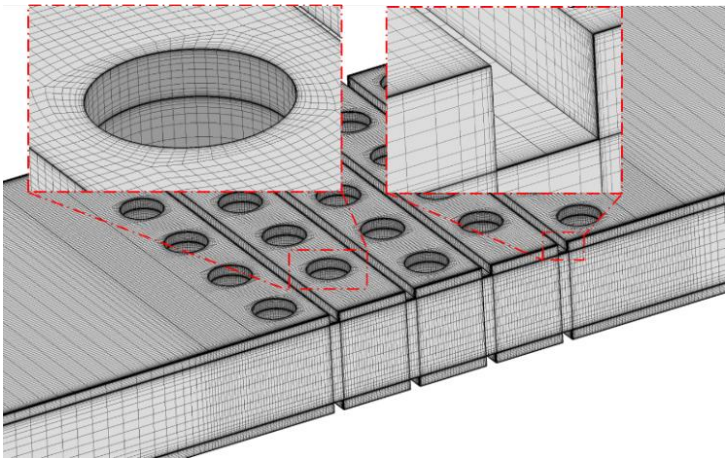

Fig. 2 Mesh structure of computational domain

2.3 Numerical methods

Using the commercial program ANSYS CFX® 19.1 (2018), the Reynolds-averaged Navier-Stokes (RANS) equations were numerically solved in this work to examine the heat transport and flow characteristics in the channel. During the validation procedure, the Shear Stress Transport (SST) turbulence model findings were contrasted with the *k-ω* turbulence model results. The *k-ω* turbulence model was applied for the remainder of the study based on this validation. The mean-squared values of the continuity, momentum, energy, and turbulent kinetic energy equations must all be smaller than 10^{-7} in order for each case to meet the convergence requirement. Along with that, the output mass flow parameter is also observed to check for convergence. ANSYS-ICEM® software is used to partition the computational domain into structured meshes for numerical simulation. The dimensionless wall distance (*y*+ value) needs to be determined less than 1 for the *k-ω* turbulence model. To meet this requirement, the mesh elements adjacent to the pin-fin surfaces and walls were set at 10-6 m. In order to improve the mesh quality for the channel, Fig. 2 depicts the mesh structure that makes use of hexagonal components and the O-grid around the pin-fins. The *k-ω* turbulence model with Reynolds number 21500 is employed, and the grid number is modified from 1.7 million to 5.0 million, in order to verify the independence of the grid.

The boundary conditions are established in accordance with Bai *et al.* (2019) guidelines. For validation, the current simulation findings are compared to their experimental and simulation outcomes. The non-slip walls encircle the channel. The surface temperature of the walls and pin-fins in the heated channel and the ribbed channel is 298.15 K, while the walls in the other regions are adiabatic. The inlet velocity is calculated based on Reynolds numbers ranging from 7400 to 36000. The inlet gas temperature is 318.15 K, and the inlet turbulence intensity is 5%. The computational domain's reference temperature is 287 K, and 1 atm of the reference pressure. The inlet is configured for dry and incompressible air. The outlet condition is specified as a static pressure of 0 Pa, and the channel is considered to be non-rotating to study the heat exchange characteristics inside the stator blade.

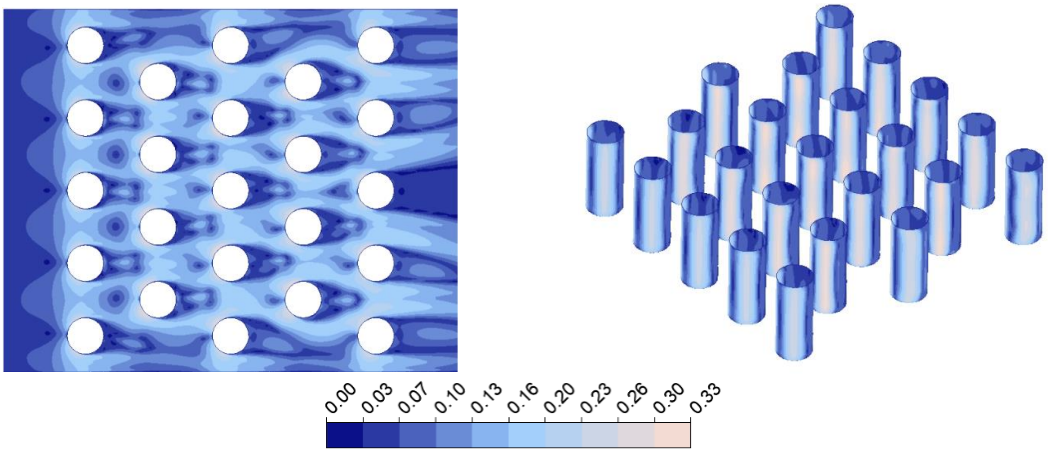

Fig. 3 Distributions of y^+ values on the surfaces of heated channel

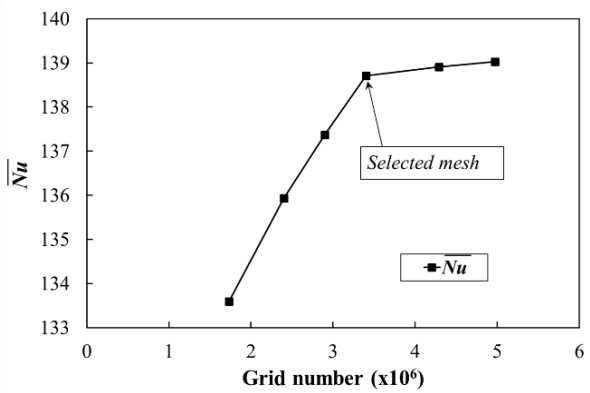

Fig. 4 Grid-dependency test for averaged Nusselt number at *Re*=21500

3. Results and discussion

3.1 Grid independence test and validation

The distributions of the dimensionless wall distance *y*+ on the endwalls and pin-fin surfaces in the heated channel with *Re*=36000 are displayed in Fig. 3. The surfaces have y^+ values less than 1, meeting the requirements of the *k*-*ω* and SST turbulence models. Thus, all remaining Reynolds numbers less than 36000 satisfy the condition of y^+ because Reynolds number is proportional to y^+. Fig. 4 displays the grid dependency test results, which indicates that the grid models with over 3.4 million meshes have the averaged Nusselt numbers that differ by less than 0.23% as compared with the case of 3.4 million meshes. Therefore, the grid with 3.4 million meshes was chosen for all remaining simulations of the work.

The results of the turbulence model test utilizing the SST and *k*-*ω* turbulence models are displayed in Table 2 and are contrasted with the experimental findings of Bai *et al.* (2019). As demonstrated in Fig. 5, the averaged Nusselt number of the heated channel grows in all circumstances when the Reynolds number does as well. These two parameters are nearly

Table 2 Comparison of numerical and experimental results

Re	$\overline{Nu}$ of Exp. data	$\overline{Nu}$ of SST	Error of SST	$\overline{Nu}$ of k-ω	Error of k-ω
7400	86.9	77.4517	-10.87%	76.7216	-11.71%
14000	106.7	104.649	-1.92%	104.575	-1.99%
21500	130.8	138.709	6.05%	135.673	3.73%
29000	158.5	170.915	7.83%	168.896	6.56%
36000	178.9	201.206	12.47%	197.566	10.43%

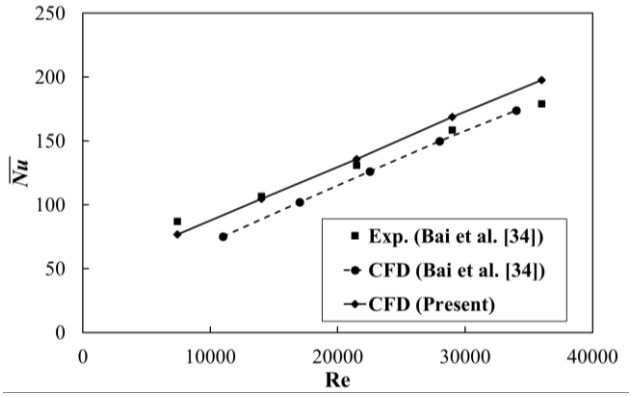

Fig. 5 Comparison of numerical and experimental results at *Re*=21500

proportionate. At Reynolds numbers 7400 and 14000, both turbulence models show similar deviations from experimantal data, but the SST model shows a slightly lower deviation. However, at *Re*≥21500, the k-ω model prevails with much lower deviations than the SST model. Specifically, at Reynolds numbers 21500, 29000 and 36000, the deviations of the SST model are 6.05%, 7.83%, and 12.47%, respectively, but those of the k-ω turbulence model are only 3.73%, 6.56%, and 10.43%, respectively. It is known that Reynolds values more than 21500 represent typical operating conditions for the gas flow within the turbine blade cooling channels. Thus, for the additional investigations, the k-ω turbulence model was used.

The averaged Nusselt number results using the k-ω turbulence model are shown in Fig. 5 along with a comparison with the experimental and numerical results of Bai *et al.* (2019) to further confirm the current numerical results. According to the visual images, the current results are comparable to the experimental data of Bai *et al.* (2019) and in the tested *Re* range, differ from their numerical results by an average of only 6.9%. Therefore, the present numerical results are reasonably validated.

The *Nu* contours on the top heated endwall at *Re*=21500 are shown in Fig. 6. As seen in Figs. 6 and 7, the frontal parts of the pin-fins are covered in the high heat transfer and high velocity regions. Horseshoe vortexes (HV) are the vortices that result from the flow and pin-fins interacting. The flow accelerates when it crosses the separation point after crossing the forward stagnation point. The wake vortices occur downstream of each pin-fin because a portion of the fluid close to the fins lacks the momentum to overcome the negative pressure differential. Low heat transfer zones are produced by these local vortices, which are trapped at each pin-fin and do not contact with the working fluid instead constantly interacting with the pin-fin and endwall surfaces (Effendy *et al.* 2019).

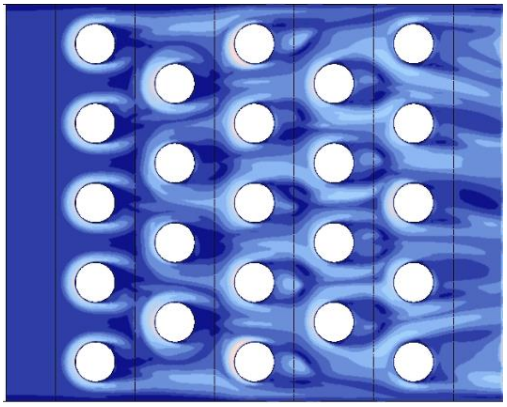

Fig. 6 Nu contours on the upper heated wall at *Re*=21500

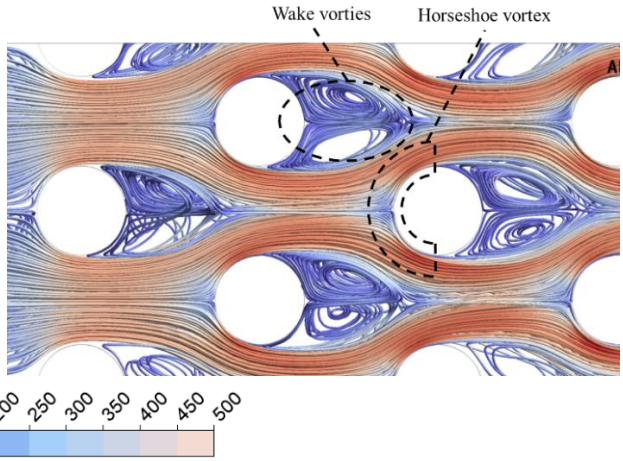

Fig. 7 Streamline flow near the endwall at *Re*=21500 from top view

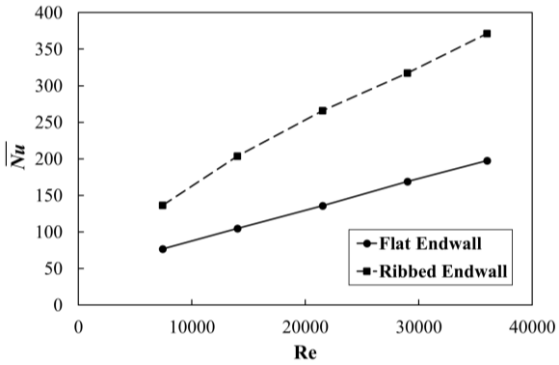

(a) Nusselt number

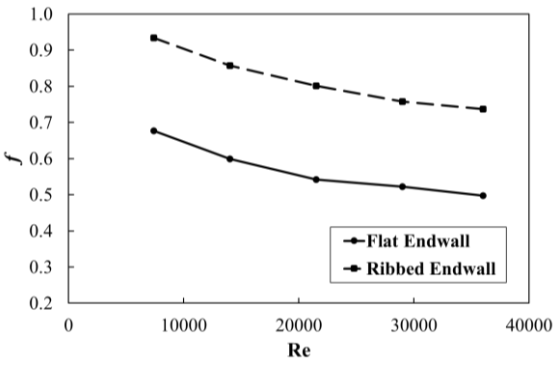

(b) Friction factor

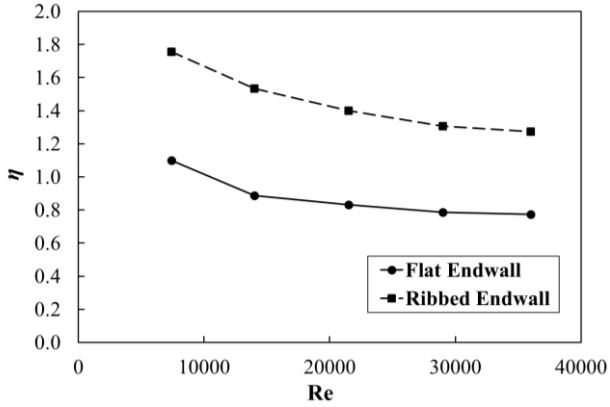

(c) Heat transfer efficiency index

Fig. 8 Comparison between the cases with flat endwalls and ribbed endwalls

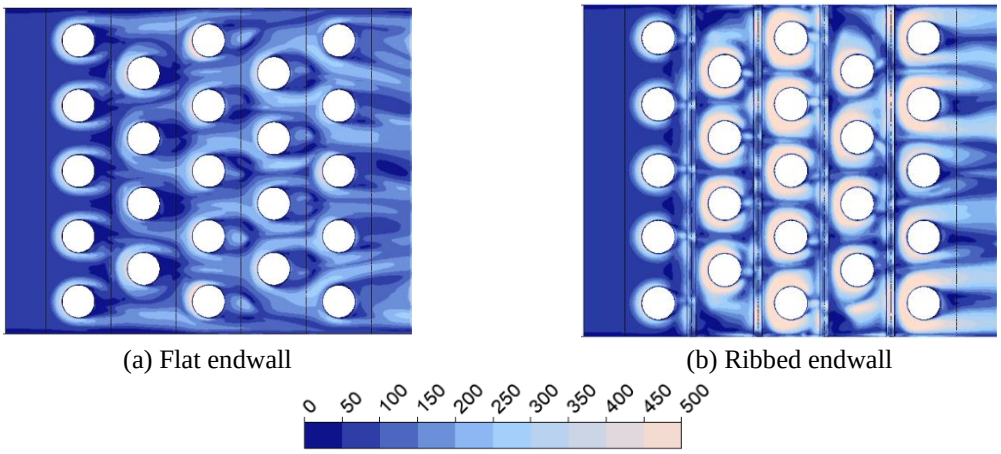

Fig. 9 Nusselt number contours on flat and ribbed endwalls in heated channel at *Re*=21500

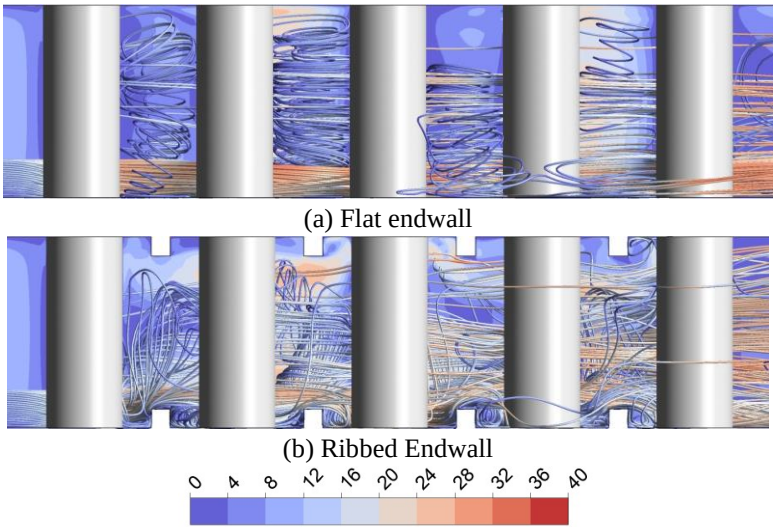

Fig. 10 Velocity contours at the middle section and streamlines near an endwall of the heated channel at *Re*=21500

3.2 Flow behaviors in a channel with ribbed endwalls

Fig. 8 compares averaged Nusselt number, friction factor (f), and HTEI (η) for two examples with flat endwalls and ribbed endwalls. For every tested Reynolds number, the ribbed endwalls' average Nusselt number is noticeably higher than the flat endwalls. Specifically, at *Re*=7400, 14000, 21500, 29000, and 36000, the averaged Nusselt number shows an increase of 78%, 95%, 96%, 88% and 88%, respectively. Along with that, the ribbed endwalls also increase the friction factor. At *Re*=7400, 14000, and 29000, the friction factor increases by 38%, 43%, and 45%, respectively. Furthermore, with the last two Reynolds values of 14000 and 21500, the maximum friction factor is 48%. Because of the ribbed endwalls, the flow is narrowed at the ribbed position, creating a lot of flow obstruction, thus causing higher pressure loss. The reduced variation of η,

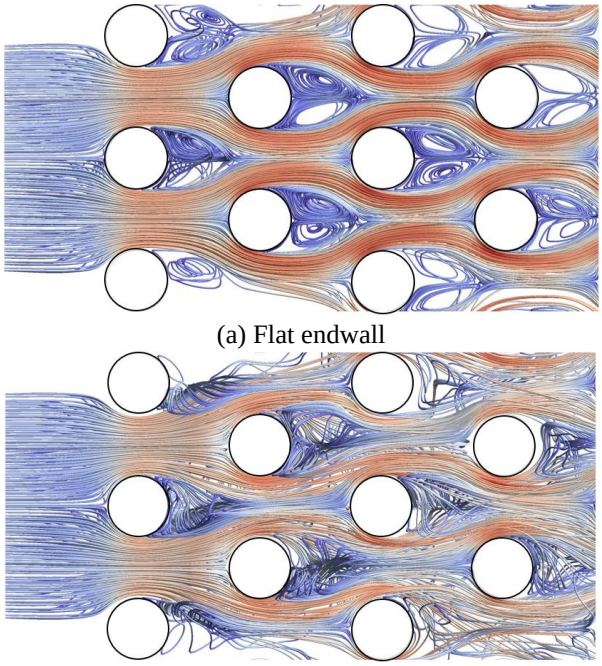

(a) Flat endwall

(b) Ribbed Endwall

Fig. 11 Streamline flow near the endwall of the channel at *Re*=21500 from top view

which is 60% to 73% higher than that of flat endwalls, is generally the result of the higher increase in $\overline{Nu}$ at the bigger Re being largely repressed by the higher increase in f at the larger Re when endwalls are ribbed. Specifically, the overall gains of η are 60%, 73%, 68%, 66%, and 65% at *Re*=7400, 14000, 21500, 29000 and 36000, respectively.

The Nusselt number distributions on the flat and ribbed endwalls of the heated channel at *Re*=21500 are displayed in Fig. 9. In the case of ribbed endwalls, the horseshoe vortices at the pin-fins are extended. In addition, the averaged Nusselt number in a HV region and surrounding regions is higher than that of flat endwalls. Fig. 10 shows regions of almost no wake vortices in locations around the region anterior to the rib rows. Besides, the wake vortices area behind the pin-fins is significantly reduced. In addition, the ribbed rows show flow-disturbing properties that help the flow better interact with the pin-fins. That's why the ribbed endwalls have better heat transfer performance than flat endwalls.

The HVs of the pin-fins (Fig. 9(b)) extend to the faces of the lateral pin-fins as well as to the flow directions. This is explained by the faster flow across the rib rows, which widens the posterior fin row's HV and increases turbulent kinetic energy. Additionally, it is discovered that in Fig. 9(b), the local vortices behind the pin-fins vanish. This is because when the flow near the endwall passes through the fins, a portion of the flow tends to move upward, disrupting wake vortices behind the pin-fins. In addition, the interaction of the flow with the endwalls, as well as the pin-fin rows, is evident by the appearance of interactive vortices. These vortices have high velocities along with continuous interaction with both the endwalls and the pin-fins which increases the heat transfer efficiency of the channel (Fig. 10(b)).

The appearance of the wake vortex regions behind the pin-fins with the flat endwalls is clearly

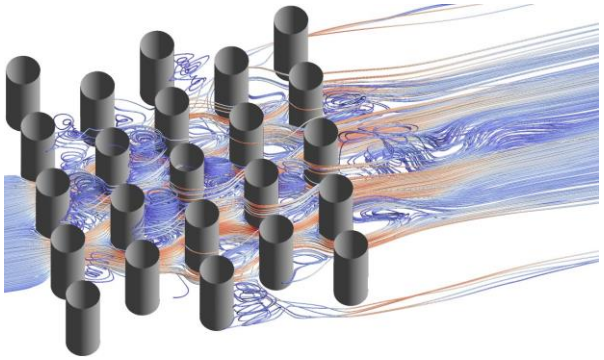

(a) Flat endwall

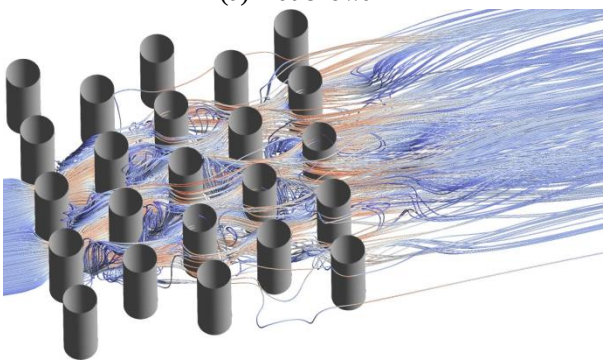

(b) Ribbed Endwall

Fig. 12 3D streamlines near the endwall in the heated channel and outlet channel at *Re*=21500

visible in Figs. 10(a) and 11(a). The appearance of ribs between the pin-fin rows makes break up these vortices because when the flow passes through the ribs, compared to wake vortices, it produces upward flows that are faster and more energetic. Thus, the wake vortices disappear in the case of the ribbed endwalls, replaced by the appearance of upward flows behind the pin-fins. As seen in Figs. 10(b) and 11(b), these flows eliminate the wake vortices behind the pin-fins. Fig. 12 illustrates the flow in the outlet channel after passing through the heated channel. The flow spreads more widely when endwalls are ribbed than when endwalls are flat. The flow passes through the ribs at the heated wall. Some of the flow splits off from the area close to the wall and combines with the flow in the center of the channel, creating distinct air flows in each direction.In addition, in the case of ribbed endwalls, the reduction of the wake vortex area behind pin-fin row 5 also makes the rear airflow more even. When ribbed endwalls are used instead of flat endwalls, the channel's heat transmission efficiency is increased for the reasons mentioned above.

3.3 Effect of the height of ribbed endwalls on heat transfer performance

To investigate the influence of geometrical parameters (Table 1), the height of the rib *Hr* is investigated first at *Re*=21500. The height ratio *Hr/H* is considered as the variable parameter where *Hr* has a value in a range from 5% to 20% of H with a step of 2.5%, and 10% is the reference value. $\overline{Nu}$ and η rose when the height ratio grew from 5% to 10%. And, from about 10% to 20%, $\overline{Nu}$ increases but η decreases as shown in Fig. 13. The maximum value of η, 1.4, is

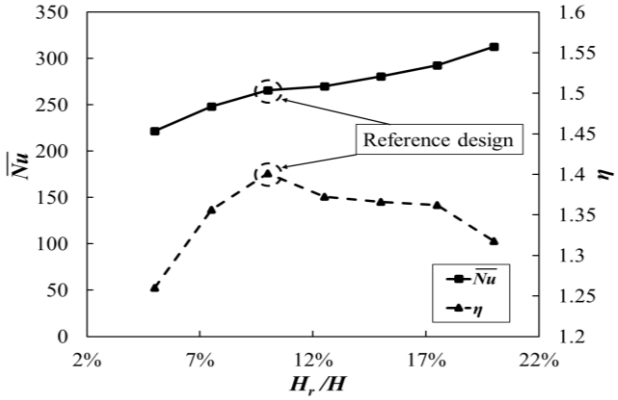

Fig. 13 Variations in the heat transfer efficiency index and Nusselt number with the ribbed endwall height at *Re*=21500

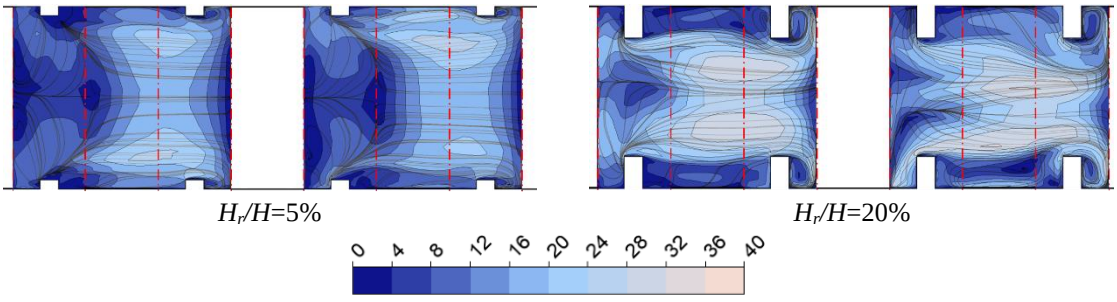

(a) Streamline flow and velocity contours

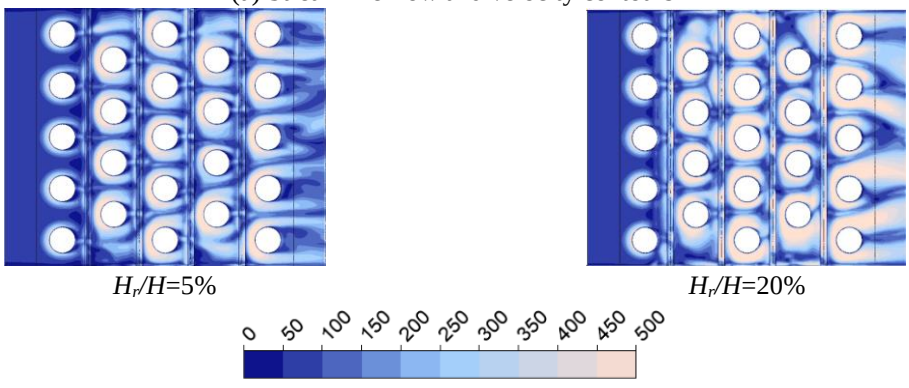

(b) Nusselt number

Fig. 14 *Nu* contours and velocity fields on the heated wall at *Re*=21500 for height ratios of 5% and 20%

achieved at the reference design. The difference between this figure and the flat endwalls instance is around 68%.

The velocity field in Fig. 14(a) reveals that, in comparison to the situation of *Hr/H*=5%, the *Hr/H*=20% exhibits higher velocity in the positions of row 2 and 4. The channel cross-section through the rib is narrowed leading to an increase in kinetic energy and velocity of the flow. As illustrated in Fig. 14, an increase in rib height causes increases in the heat transfer capacity at

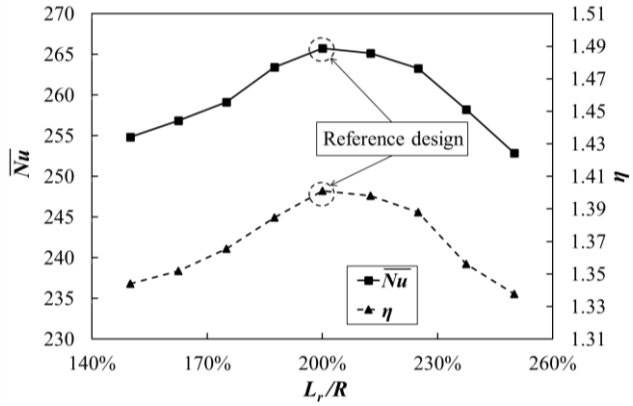

Fig. 15 Variations in the heat transfer efficiency index and Nusselt number according to the location of the ribbed endwalls at *Re*=21500

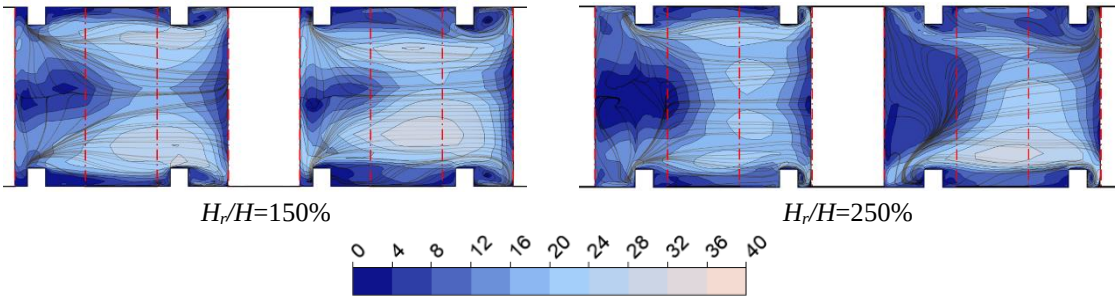

(a) Streamline flow and velocity contours

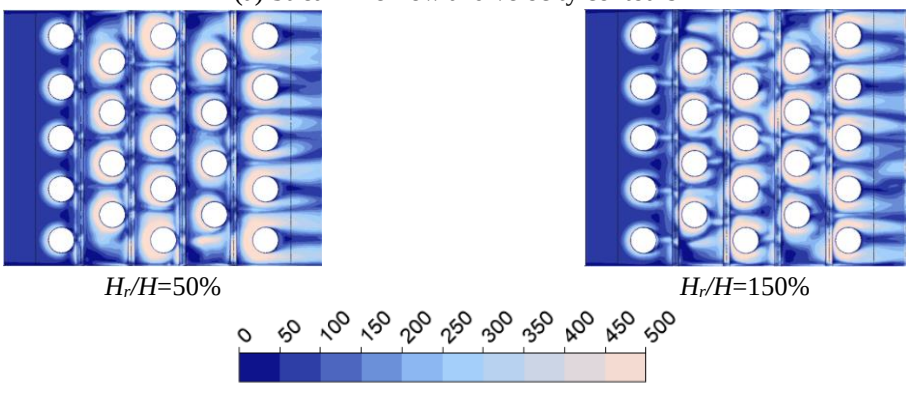

(b) Nusselt number

Fig. 16 *Nu* contours and velocity fields on the upper heated wall at 50% and 150% position ratios at *Re*=21500

every row in the channel. Fig. 14(b) shows that the overall Nusselt number at the endwalls increases as the HVs are enlarged and the Nusselt number at the HVs increases due to increased height. Additionally, the channel's converging and diverging geometries distort the flow and cause it to become less uniform. As a result, the flow tends to converge closer to the endwalls, increasing heat transfer in these areas. This can be clearly seen in the interactive vortices for *Hr/H*=20%,

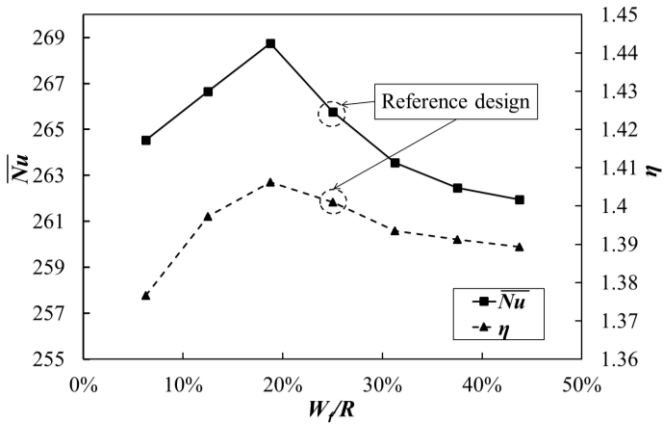

Fig. 17 Variations of heat transfer efficiency index and Nusselt number for *Wf/R* of 6.25% to 43.75% at *Re*=21500

which has a larger size and velocity than those of *Hr/H*=5%. The HTEI of the channel drops when the increase in the friction factor exceeds the rise in the averaged Nusselt number because the narrow channel also results in a significant pressure loss and a larger friction factor.

3.4 Effect of the position of ribbed endwalls on heat transfer performance

In this section, the position parameter (Table 1) in the x direction of the ribbed row (L_r) is studied. The ratio L_r/R is considered as a variable parameter where L_r has a value from 150% to 250% of H with a step of 12.5%, and the reference design is 200%. The fluctuations of $\overline{Nu}$ and η with the ratio L_r/R are displayed in Fig. 15. It is found that at the reference ratio, $\overline{Nu}$ and η are the highest. Both the graphs of Nusselt number and HTEI show the same qualitative variation and have the peaks at the reference design L_r/R=200%.

It is found that the cases L_r/R=150% and L_r/R=250% show clearly different HV shapes. The HVs expand to the upstream but narrow to the downstream in the cases of L_r/R=250%, but in the case of L_r/R=150%, on the contrary, the HVs tend to expand to the downstream and narrow to the upstream (Fig. 16(b)). Furthermore, there is less flow interaction between the ribbed row and the pin-fin row when the ribbed row position is too near or too far from the pin-fin row. The interactive pin-fin row vortex field is shown in Fig. 16(a). It is clear from the results that the endwalls function at their best when L_r/R=200% (the reference design) is used, as this design has the maximum heat transfer efficiency index (HTEI) for the channel.

3.5 Effect of the forward width of ribbed endwalls on heat transfer performance

In addition to the position and height parameters (Table 1), the width of the rib row section is investigated here. For the forward width of the rib (W_f), dimensionless parameter W_f/R is used. The W_f/R ratio is investigated from 6.25% to 43.75% with a step of 6.25%, and the reference design is 25%. For convenience in the process of manufacturing and processing parts, the ratio W_f/R and step are considered to choose the appropriate value, and then the W_f value is in a range of 0.25 mm to 1.75 mm with a step of 0.25 mm. The fluctuations of $\overline{Nu}$ and η with the ratio W_f/R are displayed

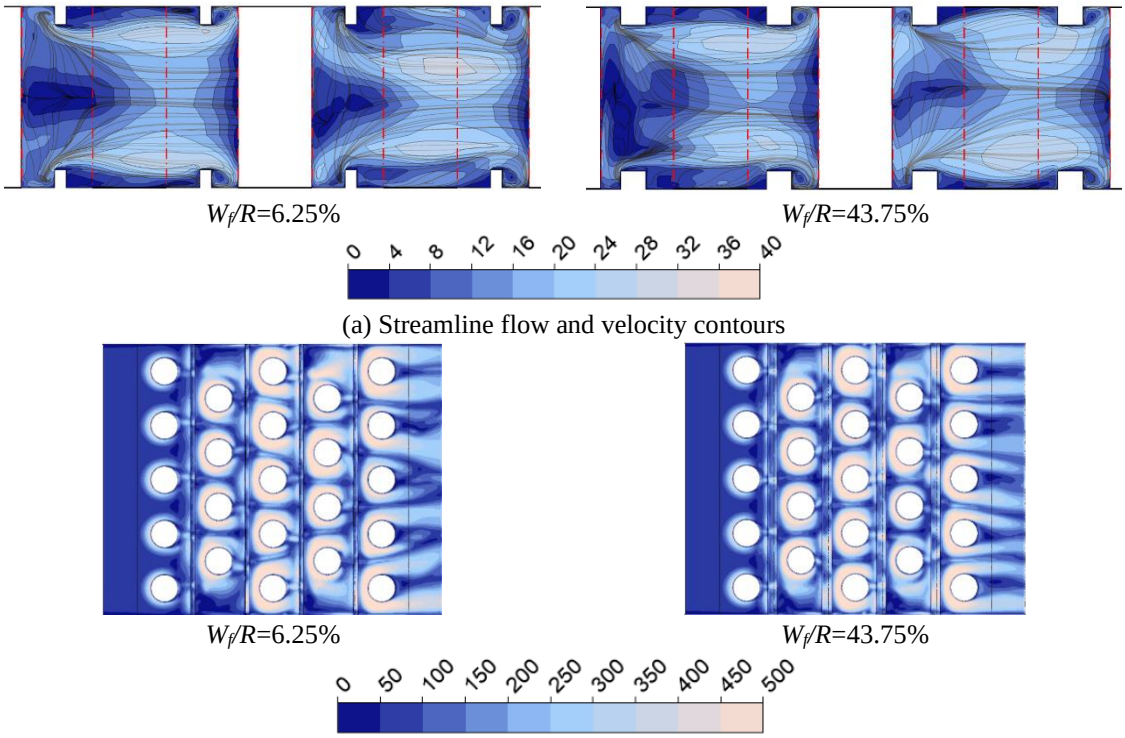

(a) Streamline flow and velocity contours

(b) Nusselt number

Fig. 18 Overheated wall velocity field and Nu contours for W_f/R of 6.25% and 43.75% at Re=21500

in Fig. 17. It is found that both $\overline{Nu}$ and η graphs reach their maximum values at the position of W_f/R=18.75%. Specifically, $\overline{Nu}$ increases by 1.13% and η increases by 0.4% at this position, as compared to the reference design. The increased width ahead of the rib row causes a narrowing of the flat walls. As a result, there is limited contact between the flow and the flat walls since the flow hasn't had enough time to interact with the ribs before it encounters the next row of ribs. As a result, as Fig. 18(a) shows, the heat transmission efficiency index decreases. On the other hand, when the rib width decreases forward, the pin-fins row and rib spacing increase, which reduces the flow contact between them. Fig. 18(b) shows that the local vortices for W_f/R=6.25% show larger area than those for W_f/R=25%. Therefore, the forward width affects HTEI and W_f/R=18.75% is the optimal value which gives the best performance.

3.6 Effect of the rear width of ribbed endwalls on heat transfer performance

Along with the forward width of the ribs row, the rear width of the ribs row (W_b in Table 1) is studied in this section. Similar to W_f/R, W_b/R is surveyed from 6.25% to 43.75% with a step of 6.25%, and the reference design is 25%. This means that W_b has a value between 0.25 mm and 1.75 mm with a step of 0.25 mm. The results of surveying the rear width of the ribs row are shown in Fig. 19 for $\overline{Nu}$ and η. According to the findings, the maximum HTEI and Nusselt number are both reached in the studied range at W_b/R=31.25%.

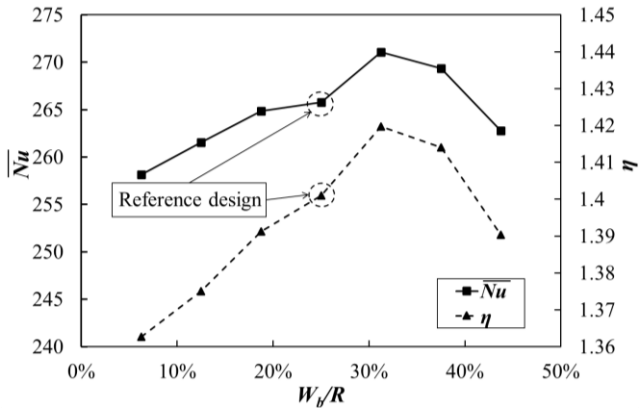

Fig. 19 Variations of Heat transfer efficiency and Nusselt number for W_b/R of 6.25% to 43.75% at Re=21500

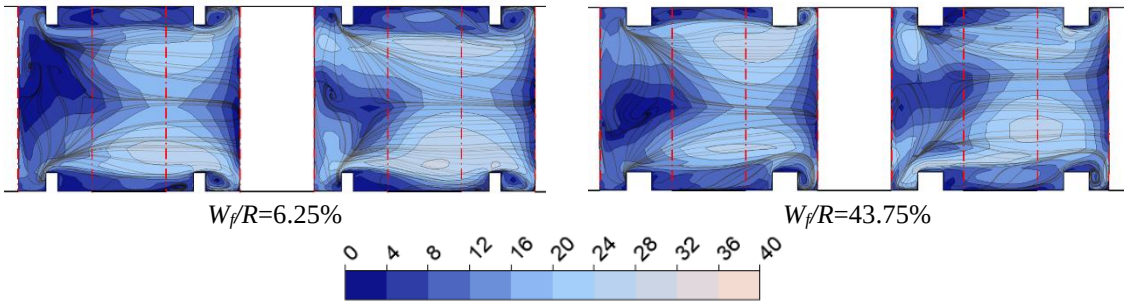

(a) Streamline flow and velocity contours

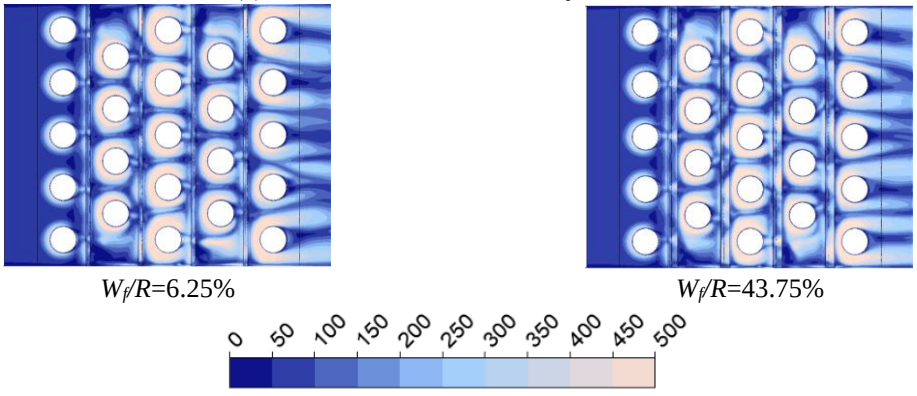

(b) Nusselt number

Fig. 20 Velocity fields and Nu contours over the heated wall for W_b/R of 6.25% and 43.75% at Re=21500

The interaction vortices between the pin-fins and the rib rows are depicted in Fig. 20(a). Because the velocities of these interactive vortices in the 43.75% example are larger than those in the 6.25% case, the 43.75% instance exhibits superior flow interaction with the endwall. Besides, Fig. 20(b) shows that in the case of 43.75% the area of the HV is narrowed to the upstream compared with the case of 6.25%. This happens as a result of the horseshoe vortex's extension towards the rib rows and the flat walls' narrowing in front of the pin-fin row. Thus, W_b/R=31.25%

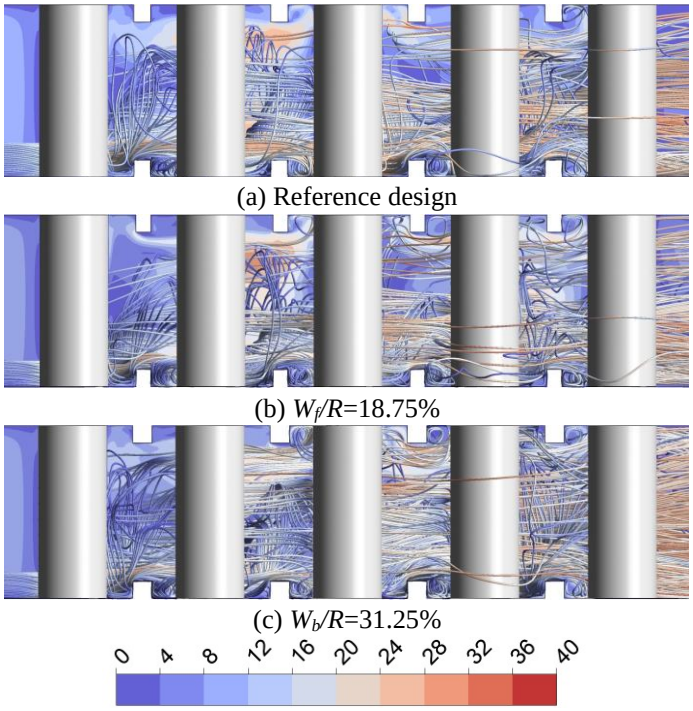

(a) Reference design

(b) W_f/R=18.75%

(c) W_b/R=31.25%

Fig. 21 Velocity contours at the middle section and streamlines near the endwall for the reference design and the best cases of Ribbed endwalls at *Re*=21500

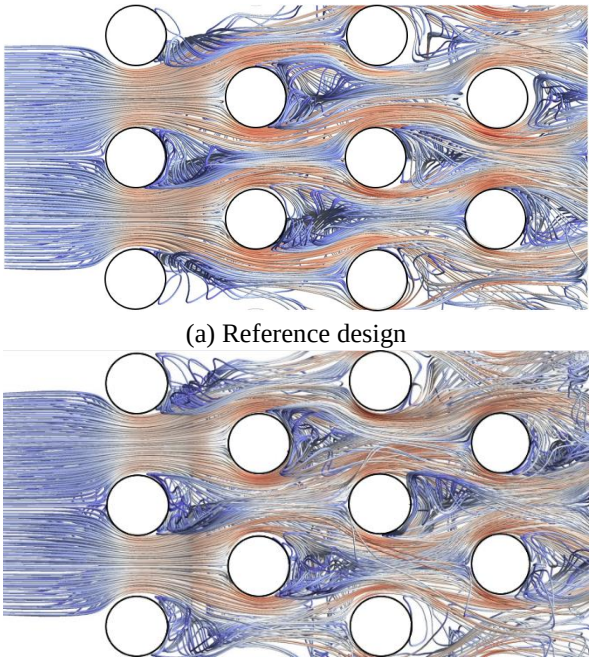

(a) Reference design

(b) W_f/R=18.75%

Fig. 22 Streamlines near the endwall of the channel from top view for the reference design and the best cases of ribbed endwalls at *Re*=21500

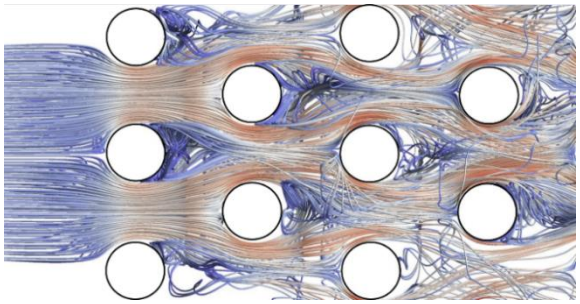

(c) W_b/R=31.25%

Fig. 22 Continued

provides optimal flow interaction with the endwalls and pin-fins, where $\overline{Nu}$ and η increase by 2% and 1.3%, respectively, as compared to the reference design.

3.7 Comparison of the reference design and the best cases of ribbed endwalls

Based on the parametric study's findings, the best improvements in heat transfer compared to the reference design are found to be obtained at W_f/R=18.75% and W_b/R=31.25%. Fig. 21 shows that in the heated channel, the flow with W_f/R=18.75% spreads wider than in the reference design. Furthermore, in the case W_f/R=18.75%, the low velocity zones behind the pin-fins in the third and fourth pin-fin rows are smaller than in the reference design, as Fig. 22 makes evident Because in the case of W_f/R=18.75% the flow in the heated channel is spread out, Fig. 23 shows that the flow in the outlet channel with W_f/R=18.75% is more uniform than that in the reference design. Another factor to consider is that the friction coefficient for W_f/R=18.75% is smaller than that of the reference design because the width of the rib is reduced. For the above reasons, the HTEI in the case W_f/R=18.75% is better than that of the reference design.

In the case of W_b/R=31.25%, the width of the ribs is widened as compared to the reference design, so the flow behind the pin-fins is pushed higher and carries more energy, which destroys the wake vortices more effectively. The flow is elevated after passing through the ribs, causing it to spread wider. This expansion aids in the more effective heat transfer within the channel as illustrated in Fig. 21(a) and 21(c). Fig. 22(a) and 22(c) show that the chaotic flow in the case of W_b/R=31.25% becomes more severe than the reference design due to the reason described above. The low velocity zones in the rear rows of pin-fins are similarly reduced, as seen in Fig. 23(a) and 23(c). From there, the improvement in HTEI for W_b/R=31.25 compared to the reference design can be explained.

4. Conclusions

In this study, RANS equations with the k-ω turbulence model in the Reynolds number range of 7400 to 36000 are used to examine the heat transfer characteristics of the ribbed endwalls in the heating channel with pin-fin arrays. The numerical results are in good agrement with the experimental data. Four geometrical parameters of the ribs with the height, position, forward width and rear width were investigated. The following conclusions are reached:

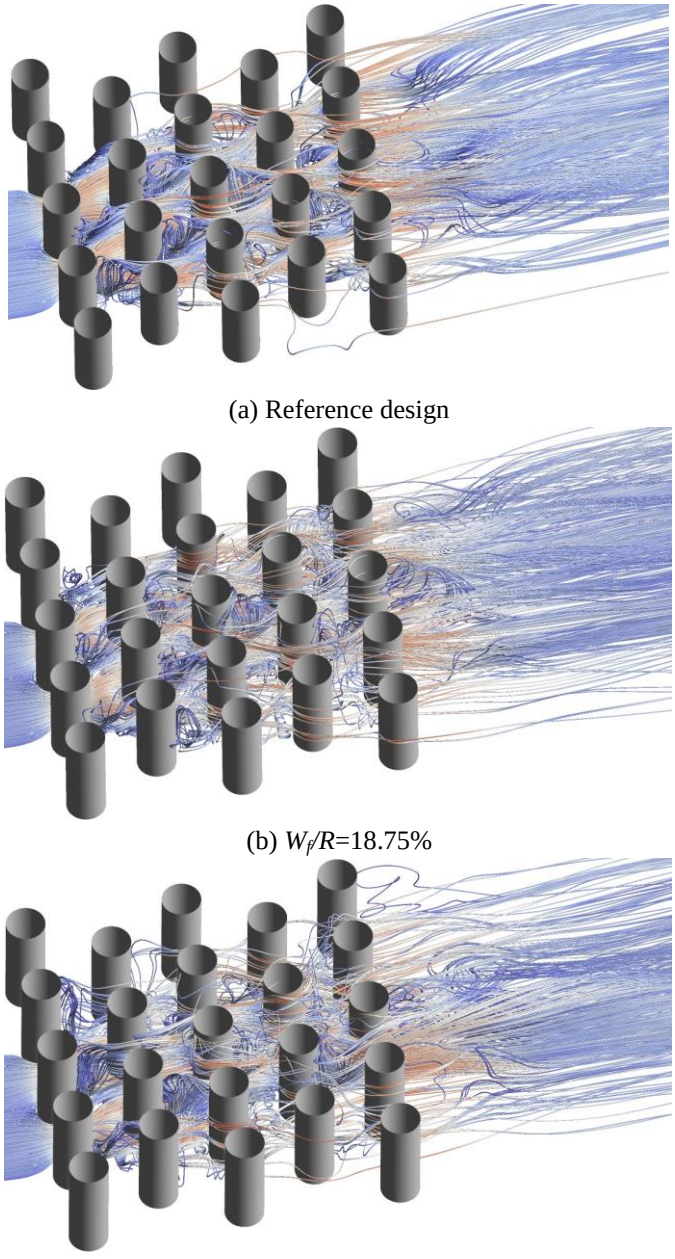

(a) Reference design

(b) W_f/R=18.75%

(c) W_b/R=31.25%

Fig. 23 3D streamlines near the endwall of the heated channel and outlet channel for the reference design and the best cases of ribbed endwalls at *Re*=21500

1. The properties of heat transmission of the ribbed endwalls are enhanced significantly as compared to the flat endwalls. In particular, when compared to the case of the flat endwalls, the ribbed endwalls demonstrate increases in the averaged Nusselt number and HTEI from 78% to 96% and 60% to 73%, respectively, at all tested Reynolds numbers.

2. The results for the flowfield show that the ribbed endwalls increase flow interaction between endwalls and pin-fins. The horseshoe vortices are expanded in all directions and the local vortices after the pin-fins being narrowed.
3. The results of the parametric study show that every examined parameter has an impact on the heat transfer performance. The performace shows maxima at the reference designs of the rib height and position parameters. For the rib width parameters, with W_f/R=18.75%, the averaged Nusselt number and HTEI increase by 1.13% and 0.4%, respectively, and with W_b/R=31.25%, they increase by 2% and 1.3%, respectively, as compared to the reference design.

Based on these findings, future research will examine different endwall geometries that further enhance heat transfer performance in channels with pin-fins, as well as refine the geometry of the ribbed endwalls utilizing optimization techniques.

Acknowledgments

This research is funded by Hanoi University of Science and Technology (HUST) under project number T2023-PC-017, and the cooperation research between HUST and Viettel Aerospace Institute (VTX).

References

ANSYS CFX-19.1 (2018), ANSYS Inc.

Axtmann, M., Poser, R., Von Wolfersdorf, J. and Bouchez, M. (2016), "Endwall heat transfer and pressure loss measurements in staggered arrays of adiabatic pin fins", *Appl. Therm. Eng.*, **103**, 1048-1056. https://doi.org/10.1016/j.applthermaleng.2016.04.066.

Bai, W., Liang, D., Chen, W. and Chyu, M.K. (2019), "Investigation of ribs disturbed entrance effect of heat transfer and pressure drop in pin-fin array", *Appl. Therm. Eng.*, **162**, 114214. https://doi.org/10.1016/j.applthermaleng.2019.114214.

Brigham, B.A. and VanFossen, G.J. (1984), "Length to diameter ratio and row number effects in short Pin-Fin heat transfer", *J. Eng. Gas Turbin. Power*, **106**(1), 241-244. https://doi.org/10.1115/1.3239541.

Chi, X., Shih, T.I.P., Bryden, K.M., Siw, S., Chyu, M.K., Ames, R. and Dennis, R.A. (2011), "Effects of pin-fin height on flow and heat transfer in a rectangular duct", *Turbo Expo: Power for Land, Sea, and Air*, **5**, 1435-1445. https://doi.org/10.1115/GT2011-46014.

Chyu, M.K. (1990), "Heat transfer and pressure drop for short pin-fin arrays with pin-endwall fillet", *J. Heat Transf.*, **112**(4), 926-932. https://doi.org/10.1115/1.2910502.

Chyu, M.K., Siw, S.C. and Moon, H.K. (2009), "Effects of height-to-diameter ratio of pin element on heat transfer from staggered Pin-Fin arrays", *Turbo Expo: Power for Land, Sea, and Air*, **3**, 705-713. https://doi.org/10.1115/gt2009-59814.

Dinh, C.T., Do, K.D.C., Chung, D.H. and Truong, H.S. (2023), "Effects of pin-fins with trapezoidal endwall on heat transfer characteristics in gas turbine blade internal cooling channels", *J. Mech. Sci. Technol.*, **37**(5), 2199-2210. https://doi.org/10.1007/s12206-023-2107-9.

Dinh, C.T., Nguyen, T.M., Vu, T.D., Park, S.G. and Nguyen, Q.H. (2021), "Numerical investigation of truncated-root rib on heat transfer performance of internal cooling turbine blades", *Phys. Fluid.*, **33**(7), 076104. https://doi.org/10.1063/5.0054149.

Dittus, F.W. and Boelter, L.M.K. (1985), "Heat transfer in automobile radiators of the tubular type", *Int. Commun. Heat Mass Transf.*, **12**(1), 3-22. https://doi.org/10.1016/0735-1933(85)90003-X.

Do, K.D.C., Chung, D.H., Tran, D.Q., Dinh, C.T., Nguyen, Q.H. and Kim, K.Y. (2022), "Numerical

investigation of heat transfer characteristics of Pin-Fins with roughed endwalls in gas turbine blade internal cooling channels", *Int. J. Heat Mass Transf.*, **195**, 123125. https://doi.org/10.1016/j.ijheatmasstransfer.2022.123125.

Effendy, M., Yao, Y.F., Yao, J. and Marchant, D.R (2019), "Detached eddy simulation of blade trailing-edge cutback cooling performance at various ejection slot angles", *Int. J. Heat Fluid Flow*, **80**. 114214. https://doi.org/10.1016/j.ijheatfluidflow.2019.10848114214.7.

Ghosh, S., Mondal, S., Kapat, J.S. and Ray, A. (2020), "Shape optimization of pin fin arrays using Gaussian process surrogate models under design constraints", *Turbo Expo: Power for Land, Sea, and Air*, **84164**, V07AT15A021. https://doi.org/10.1115/GT2020-15277.

Kirki, G. and Constantinescu, G. (2015), "Effects of cylinder Reynolds number on the turbulent horseshoe vortex system and near wake of a surface-mounted circular cylinder", *Phys. Fluid.*, **27**(7), 075102. https://doi.org/10.1063/1.4923063.

Li, P. and Kim, K.Y. (2008), "Multiobjective optimization of staggered elliptical Pin-Fin arrays", *Numer. Heat Transf., Part A: Appl.*, **53**, 418-431. https://doi.org/10.1080/10407780701632759.

Liang, C. and Rao, Y. (2021), "Numerical study of turbulent flow and heat transfer in channels with detached pin fin arrays under stationary and rotating conditions", *Int. J. Therm. Sci.*, **160**, 106659. https://doi.org/10.1016/j.ijthermalsci.2020.10665.

Metzger, D.E., Berry, R.A. and Bronson, J.P. (1982), "Developing heat transfer in rectangular ducts with staggered arrays of short pin fins", *J. Heat Transf.*, **104**(4), 700-706. https://doi.org/10.1115/1.3245188.

Moon, M.A. and Kim, K.Y. (2013), "Heat transfer performance of a new fan-shaped pin-fin in internal cooling channel", *Turbo Expo: Power for Land, Sea, and Air*, **55140**, V03AT12A006. https://doi.org/10.1115/GT2013-94193.

Ostanek, J.K. and Thole, K.A. (2012), "Effects of varying streamwise and spanwise spacing in Pin-Fin arrays", *Turbo Expo: Power for Land, Sea, and Air*, **44700**, 45-57. https://doi.org/10.1115/gt2012-68127.

Otto, M., Hodges, J., Gupta, G. and Kapat, J.S. (2019), "Vortical structures in pin fin arrays for turbine cooling applications", *Turbo Expo: Power for Land, Sea, and Air*, **58646**, V05AT16A003. https://doi.org/10.1115/GT2019-90552.

Park, J.S., Kim, K.M., Lee, D.H., Cho, H.H. and Chyu, M.K. (2008), "Heat transfer on rotating channel with various heights of Pin-Fin", *Turbo Expo: Power for Land, Sea, and Air*, **4**, 727-734. https://doi.org/10.1115/gt2008-50783.

Pham, K.Q., Nguyen, Q.H., Vu, T.D. and Dinh, C.T. (2020), "Effects of boot-shaped rib on heat transfer characteristics of internal cooling turbine blades", *J. Heat Transf.*, **142**(10), 102106. https://doi.org/10.1115/1.4047490.

Sa, K.J. and Kim, K.Y. (2015), "Analysis of flow over a gapped Pin-Fin", *Proceedings of the International Symposium on Turbulence, Heat and Mass Transfer*, September. https://doi.org/10.1615/ichmt.2015.thmt-15.2010.

Sa, K.J., Afzal, A. and Kim, K.Y. (2017), "Performance analysis and design optimization of gapped Pin-Fin in a cooling channel", *Heat Transf. Eng.*, **39**(6), 549-567. https://doi.org/10.1080/01457632.2017.1320170.

Sahin, B., Ozturk, N.A. and Gurlek, C. (2008), "Horseshoe Vortex Studies in the passage of a model plate-fin-and-tube heat exchanger", *Int. J. Heat Fluid Flow*, **29**(1), 340-351. https://doi.org/10.1016/j.ijheatfluidflow.2007.06.005.

Sahiti, N., Lemouedda, A., Stojkovic, D., Durst, F. and Franz, E. (2006), "Performance comparison of pin fin in-duct flow arrays with various pin cross-sections", *Appl. Therm. Eng.*, **26(**11-12), 1176-1192. https://doi.org/10.1016/j.applthermaleng.2005.10.042.

Schekman, S. and Kim, T. (2017), "Thermal flows around a fully permeable short circular cylinder", *Int. J. Heat Mass Transf.*, **105**. 196-206. https://doi.org/10.1016/j.ijheatmasstransfer.2016.09.089.

Sircar, A., Kimber, M., Rokkam, S. and Botha, G. (2020), "Turbulent flow and heat flux analysis from validated large eddy simulations of flow past a heated cylinder in the near wake region", *Phys. Fluid.*, **32**(12), 125119. https://doi.org/10.1063/5.0031831 .

Siw, S.C., Fradeneck, A.D., Chyu, M.K. and Alvin, M.A. (2015), "The effects of different pin-fin arrays on

heat transfer and pressure loss in a narrow channel", *Turbo Expo: Power for Land, Sea, and Air*, **56727**, V05BT13A026. https://doi.org/10.1115/gt2015-43855.

Sparrow, E.M., Ramsey, J.W. and Altemani, C.A.C. (1980), "Experiments on in-line pin fin arrays-and performance comparisons with staggered arrays", *Adv. Heat Transf.*, **102**(1). 44-50. https://doi.org/10.1115/1.3244247.

Tang, T., Yu, P., Shan, X., Li, J. and Yu, S. (2020), "On the transition behavior of laminar flow through and around a multi-cylinder array", *Phys. Fluid.*, **32**(1), 013601. https://doi.org/10.1063/1.5132362.

Tran, V.H., Nguyen, T.H., Plourde, F., Do, K.D.C., Chung, D.H., Dinh, C.T. and Pham, G.D. (2023), "Investigation of extruded endwall on heat transfer characteristics of channel with staggering pin-fins", *Int. J. Fluid Mach. Syst.*, **16**(02), 169-183. https://doi.org/10.5293/IJFMS.2023.16.2.169.

Uzol, O. and Camci, C. (2001), "Elliptical pin fins as an alternative to circular pin fins for gas turbine blade cooling applications, Part 2: Wake flow field measurements and visualization using particle image velocimetry", *Turbo Expo: Power for Land, Sea, and Air*, **78521**, V003T01A057. https://doi.org/10.1115/2001-GT-0181.

Wan, W., Deng, D., Huang, Q., Zeng, T. and Huang, Y. (2017), "Experimental study and optimization of pin fin shapes in flow boiling of micro pin fin heat sinks", *Appl. Therm. Eng.*, **114**, 436-449. https://doi.org/10.1016/j.applthermaleng.2016.11.182.

Won, S.Y., Mahmood, G.I. and Ligrani, P.M. (2004), "Spatially-resolved heat transfer and flow structure in a rectangular channel with Pin Fins", *Int. J. Heat Mass Transf.*, **47**(8-9), 1731-1743. https://doi.org/10.1016/j.ijheatmasstransfer.2003.10.007.

Ye, L., Liu, Z., Gao, C., Yang, X. and Feng, Z. (2017), "Numerical study on heat transfer perfor mance of a new-proposed Pin-Fin in an internal channel", *Turbo Expo: Power for Land, Sea, and Air*, **50879**, V05AT11A014. https://doi.org/10.1115/gt2017-64573.

Zukauskas, A. (1972), "Heat transfer from tubes in cross flow", *Adv. Heat Transf.*, **08**, 93-160. https://doi.org/10.1016/S0065-2717(08)70038-8.

AP